SCIENCE CHINA
Chemistry

•ARTICLES•

May 2021 Vol.64 No.5: 852–860
https://doi.org/10.1007/s11426-020-9950-8

Concentrated hydrogel electrolyte for integrated supercapacitor with high capacitance at subzero temperature

Yang Bai[1], Rong Liu[2*], Yang Liu[1], Yuanming Wang[1], Xue Wang[1], Huanhao Xiao[1] & Guohui Yuan[1*]

[1]*MIIT Key Laboratory of Critical Materials Technology for New Energy Conversion and Storage, School of Chemistry and Chemical Engineering, Harbin Institute of Technology, Harbin 150001, China;*
[2]*Ocean College, Hebei Agricultural University, Qinhuangdao 066000, China*

Received November 22, 2020; accepted January 29, 2021; published online March 29, 2021

Hydrogel electrolytes with anti-freezing properties are crucial for flexible quasi-solid-state supercapacitors operating at low temperatures. However, the electrolyte freezing and sluggish ion migration caused by the cold temperature inevitably damage the flexibility and electrochemical properties of supercapacitors. Herein, we introduce the concentrated electrolyte into a freeze-casted poly(vinyl alcohol) hydrogel film not only reducing the freezing point of the electrolyte (−51.14 °C) in gels for ensuring the flexibility, but also improving the ionic conductivity of the hydrogel electrolyte (5.92 mS cm^{-1} at −40 °C) at low temperatures. As a proof, an all-in-one supercapacitor, synthesized by the one-step polymerization method, exhibits a good specific capacitance of 278.6 mF cm^{-2} at −40 °C (accounting for 93.8% of the capacitance at room temperature), high rate performance (50% retention under the 100-fold increase in current densities), and long cycle life (88.9% retention after 8,000 cycles at −40 °C), representing an excellent low-temperature performance. Our results provide a fresh insight into the hydrogel electrolyte design for flexible energy storage devices operating in the wide range of temperature and open up an exciting direction for improving all-in-one supercapacitors.

anti-freezing hydrogel, ionic conductivity, all-in-one, flexible supercapacitors

Citation: Bai Y, Liu R, Liu Y, Wang Y, Wang X, Xiao H, Yuan G. Concentrated hydrogel electrolyte for integrated supercapacitor with high capacitance at subzero temperature. *Sci China Chem*, 2021, 64: 852–860, https://doi.org/10.1007/s11426-020-9950-8

1 Introduction

Driven by the potential application of energy storage devices in emerging flexible and wearable electronics, recent research efforts have been directed towards improving their mechanical properties and electrochemical stability under a wide temperature range [1]. Among various energy storage devices, flexible supercapacitors attract an ever-growing interest owing to their ultra-long cycle life, fast charge-discharge speed, and high power density [2,3]. In particular, quasi-solid-state supercapacitors are suitable for human body to wear because of the device safety upon repetitively mechanical deformation [4,5]. Generally, a flexible quasi-solid-state supercapacitor is mainly composed of two flexible electrodes (serving as anode and cathode, respectively) and hydrogel electrolytes (also used as a separator) [6]. However, the sensitivity of hydrogel electrolyte to the operation temperature apparently damages the electrochemical performance of supercapacitors at a frigid environment because the low temperature decelerates the ions migration rate of electrolyte [1,7,8]. Furthermore, the mechanical properties deteriorate at low temperature due to the electrolyte freezing [9]. Therefore, it is urgently needed to explore a freeze-tolerant hydrogel electrolyte to obtain an ideal flexible super-

*Corresponding authors (email: 562204852@qq.com; yghhit@163.com)

© Science China Press and Springer-Verlag GmbH Germany, part of Springer Nature 2021

capacitor with excellent electrochemical stability and superior flexibility in the frozen environment.

Hydrogel electrolytes, as one kind of prospective solid electrolytes, are commonly composed of polymeric matrix and water-dissolving electrolyte salts, exhibiting their flexibility and liquid-like ions transport characteristics [10]. However, due to the large amount of water in gels, the electrolyte freezing and sluggish ion migration are inevitable at the frigid temperature, affecting the mechanical property and electrochemical performance of hydrogel [7,9]. For overcoming this shortfall, several researchers adopt non-aqueous electrolytes with low-freezing points for low-temperature resistant supercapacitors such as acetonitrile, 1,3-dioxolane, and 1-butyl-3-methylimidazolium tetrafluoroborate ionic liquid [1,11,12]. Nevertheless, most non-aqueous electrolytes have toxic, flammable, and complex preparation process, leading to potential safety hazards to users [7]. Recently, some studies introduce low-molecular organic compounds into gels (such as ethylene glycol [13–15], glycerol [16,17], and dimethyl sulfoxide [18]) displacing some water to form organic hydrogels, which can decrease the freezing point of electrolyte and remain ionic conductivity at subzero temperatures. But the increased viscosity of the mixed solvents lowers the electrolyte ions migration rate, which is adverse for high power output [19–21]. Besides, some inorganic salts are used to depress the freezing point of solution in gels, but the as-prepared hydrogels cannot be directly used in flexible quasi-solid-state supercapacitor with different electrolytes (acid, alkaline, and neutral) [22,23]. Thus, a desirable anti-freezing hydrogel with high ionic conductivity and superior mechanical properties is essential for quasi-solid-state supercapacitors to remain electrochemical activity at low temperatures. Inspired by the aqueous proton battery, the concentrated electrolyte is able to reduce the freezing point of electrolyte avoiding the electrolyte freezing, thus ensuring the devices exhibit excellent flexibility [9]. Furthermore, the concentrated electrolyte facilitates electrolyte ions reaching to the electrode surface, thereby alleviating the slow migration caused by low temperature [9,19]. Therefore, we deem that the hydrogel with concentrated electrolyte can promote the quasi-solid-state supercapacitor obtaining high performance at low temperatures.

Herein, we report an anti-freezing hydrogel electrolyte by infusing concentrate electrolyte into the lyophilized poly (vinyl alcohol) (PVA) hydrogel. The freezing-tolerant hydrogel exhibits excellent mechanical properties (rolling, bending, twisting, folding and compressing at −40 °C), low freezing point (−51.14 °C), and high ionic conductivity (5.92 mS cm^{-1} at −40 °C). Generally, most quasi-solid-state supercapacitors are assembled in a multilayer laminated construction, in which a hydrogel electrolyte supports flexible electrode materials [24]. Based on this assembling mode, a large interface resistance comes out due to the multilayer laminated configuration inhibiting the fast transfer of ions and charge, and the resistance increases under consecutive bending cycles resulting in poor electrochemical stability [25,26]. The all-in-one configuration is one promising approaching for the deformable stability, which directly synthesizes electrode materials on the surface of hydrogel electrolyte. [25] Thus, the low-temperature-resistant supercapacitor was fabricated on the anti-freezing hydrogel electrolyte with polyaniline (PANi) as electrodes. The as-prepared all-in-one supercapacitor delivers 278.6 mF cm^{-2} at 0.5 mA cm^{-2} at −40 °C, accounting for 93.8% of the specific capacitance (296.9 mF cm^{-2}) at room temperature (RT). Furthermore, the capacity retention of flexible supercapacitor can reach 50% under the 100-fold increase in current densities, along with stable electrochemical performance under deformation states and long cycle life (remain 88.9% after 8000 cycles at −40 °C).

2 Experimental

2.1 Synthesis of f-PVA hydrogel and all-in-one supercapacitors

Preparation of f-PVA. The f-PVA was fabricated by a lyophilization process after synthesizing a chemical cross-linked PVA. Firstly, 2 g of PVA (M_w=1799) was added into 20 mL of the H_2SO_4 solution (1 mol L^{-1}) and the mixture was stirred at 90 °C until the solution became clear. After cooling, 2 mL of the glutaraldehyde (2 vol%) was added into the above solution, and followed by transferring into a Petri dish (diameter, d=9 cm) and standing until it lost fluidity. Subsequently, the obtained PVA hydrogel was soaked in deionized water overnight and then freeze-dried for 4 h, and the as-prepared film was marked as f-PVA. Then, f-PVA hydrogel electrolyte was obtained by immersing f-PVA films into different concentrations of H_2SO_4 solutions. The resulting hydrogels were labeled as f-PVA1, f-PVA2 and f-PVA3, where 1, 2, and 3 represent the molar concentration of soaked H_2SO_4 solution.

Fabrication of the all-in-one configured PANi-f-PVA supercapacitor. PANi electrodes were decorated onto the surface of f-PVA by chemical oxidation polymerization. At first, 1460 μL of the aniline monomer was dissolved in 20 mL of the HCl solution (1 mol L^{-1}) to form solution A, and then a piece of f-PVA with a square shape (20 mm length × 20 mm width) was placed into the solution A. 5.48 g of ammonium persulfate was dissolved into another 20 mL of the HCl solution (1 mol L^{-1}) to form solution B. After that, the solution B was dropped into solution A (pre-cooled to 0 °C) under vigorous stirring, and the mixed solution was kept in ice-water bath (0–4 °C) for 8 h. After completing the polymerization, the as-prepared PANi-f-PVA film was washed

with acetone and deionized water three times in turn. The PANi-f-PVA supercapacitor was obtained by cutting the film into a square piece with 15 mm length×15 mm width and immersing in 3 mol L^{-1} H_2SO_4 electrolyte for 24 h, and the sample was marked as PANi-f-PVA3. For the best performance of the capacitor, the optimum loading amount of PANi electrode was controlled by adjusting the initial concentration of aniline monomer. Besides, for comparison, two PANi-f-PVA films were respectively soaked in 1 and 2 mol L^{-1} H_2SO_4, and marked as PANi-f-PVA1 and PANi-f-PVA2, respectively.

2.2 Characterization

Characterization measurements. In the scanning electron microscopy (SEM, Zeiss, Germany) test, the samples were firstly frozen for 48 h and freeze-dried in a lyophilization instrument. Then the surface and the cross-section morphologies of f-PVA and PANi-f-PVA were observed by SEM. Functional groups of f-PVA and PANi-f-PVA were tested by Fourier transform infrared spectroscopy (FT-IR, Thermo, USA). The freezing point of f-PVA3 hydrogel electrolyte was confirmed with the differential scanning calorimetry (DSC) by cooling down to −70 °C at a rate of 5 °C min^{-1}. After cutting the gels into a rectangle shape (10 mm length×30 mm width), the stress-strain curves of PVA and f-PVA*x* were carried out at a stretch rate of 2 mm min^{-1}. The elastic tests were tested by dynamic mechanical analysis (DMA) measurement (TA Instrument Q800, USA) at RT and −40 °C, with a strain of 80 %, and the sample size is a cylinder with a height of 10 mm and a diameter of 10 mm.

Electrochemical performance. In this work, the electrochemical measurements of capacitors were carried out in the two-electrode system, and the samples were encapsulated before test. The cyclic voltammetry (CV) tests were carried out at a voltage of 0–0.8 V at the sweep rate of 1–50 mV s^{-1}. The galvanostatic charge-discharge (GCD) were measured at different current density of 0.5–50 mA cm^{-2}. The electrochemical characters of hydrogels and supercapacitors were examined by electrochemical impedance spectroscopy (EIS) with platinum as current collectors at a frequency of 10^{-2}–10^{5} Hz.

3 Results and discussion

The fabrication processes of the anti-freezing hydrogel and the all-in-one supercapacitor are illustrated in Figure S1 (Supporting Information online). For a start, the PVA hydrogel film was synthesized by the aldol condensation from glutaraldehyde and PVA by using H_2SO_4 as a catalyst (Figure S2(a)). In this way, the PVA solution loses fluidity and forms a free-standing film with transparency and flexibility (Figure S2(b, c)). The abundant hydroxyl groups in the PVA hydrogel are benefit for water retention and electrolyte ions migration [8,23]. However, the low temperature causes the electrolyte freezing, which is unfavorable for ions transfer [27]. In order to ensure the mobility of electrolyte ions in the cold temperature, the freezing point of electrolyte solution in gels can be reduced by increasing the concentration of H_2SO_4 solution [19]. Nevertheless, after being immersed in 3 mol L^{-1} H_2SO_4 solution for two weeks, the PVA hydrogel obviously decomposes indicating that the concentrated H_2SO_4 solution has an adverse effect on the stability of polymers (Figure S3) [19,27,28]. Considering the practical application, the mechanical stability of hydrogel electrolyte is necessary for supporting electrodes. The prior researches point out that the low temperature promotes the formation of crystallites in PVA gels enhancing the network structure by physical cross-links. Thus, the freeze-drying operation can be workable in the improvement of mechanical strength [15,29]. After lyophilizing, the as-prepared f-PVA gel is opaque and flexible, and the thickness of f-PVA is about 1 mm (Figure S4(a)). The SEM images of f-PVA show that the surface of f-PVA is wrinkled with a few micropores due to the water sublimation during the freeze-drying operation, and the cross-section exhibits a homogeneous and compact structure (Figure S4(b, c)) [25,30]. Given by the tensile stress-strain curves shown in Figure 1(a), the lyophilized PVA hydrogel exhibits superior mechanical strength and can sustain up to 175% stretching under a stress of 0.48 MPa, while that of PVA hydrogel is only 0.01 MPa. It can be inferred that the as-prepared free-standing PVA film is prepared by adding a little amount of glutaraldehyde, which means that a large amount of unreacted hydroxyl groups still remain in the PVA gel [25]. The freeze-drying process promotes the formation of physical cross-links of PVA gels through hydrogen bonds and Van Edward forces, and enhances the robustness of the hydrogel [29]. Then, the stability of f-PVA in concentrated H_2SO_4 solutions is further investigated by soaking f-PVA gels in 1–6 mol L^{-1} H_2SO_4 for two days (Figure S5). It shows that the f-PVA hydrogels are steady in 1–3 mol L^{-1} H_2SO_4, but degrade in 4–6 mol L^{-1} H_2SO_4, indicating that the f-PVA gel has a better acid resistance with the concentrated H_2SO_4 than that of PVA gels. Furthermore, after soaking in 3 mol L^{-1} H_2SO_4 for 30 days, the f-PVA3 gel remains stable, which means the f-PVA with concentrated electrolyte can be further studied as anti-freezing hydrogel electrolyte (Figure S6(a, b)). The mechanical robustness of f-PVA1, f-PVA2, and f-PVA3 are investigated by tensile stress-strain curves measurements, and the results are shown in Figure 1(b). Although the mechanical strength decreases with the increasing concentration of H_2SO_4, the declining trend of mechanical properties slows down when the concentration of H_2SO_4 solution increases to

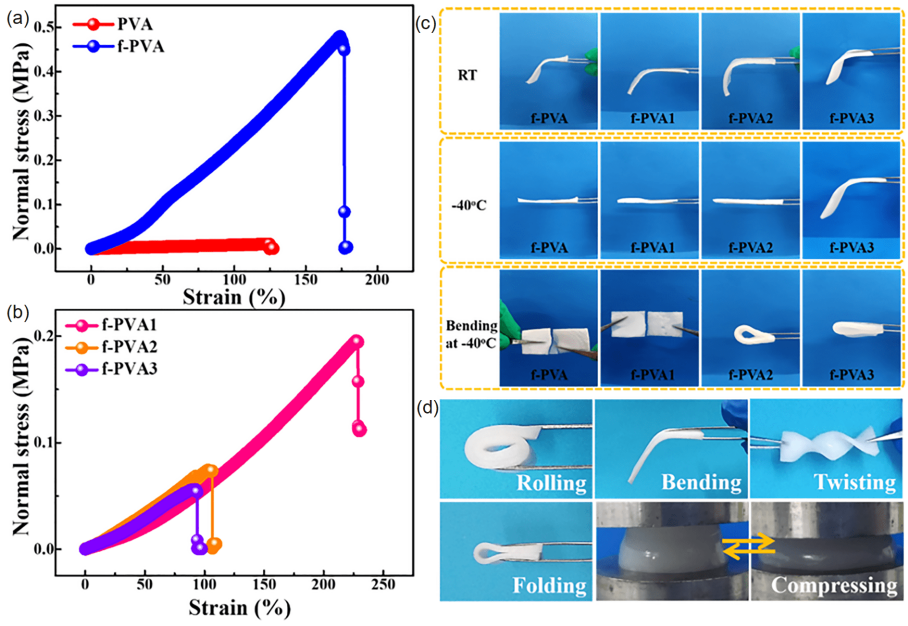

Figure 1 (a) Tensile stress-strain curves of PVA and f-PVA; (b) tensile stress-strain curves of f-PVA1, f-PVA2, and f-PVA3 hydrogels; (c) flexibility of f-PVA, f-PVA1, f-PVA2, and f-PVA3 at RT, −40 °C, and bending state at −40 °C; (d) mechanical properties of f-PVA3 after freezing at −40 °C for 24 h (color online).

3 mol L^{-1}. Besides, the flexibility of f-PVA, f-PVA1, f-PVA2 and f-PVA3 are further measured after freezing at −40 °C for 24 h. The results shown in Figure 1(c) display that f-PVA and f-PVA1 can be easily broken up while f-PVA2 and f-PVA3 are still flexible. Moreover, Figure 1(d) shows that f-PVA3 gels frozen at −40 °C can be easily rolled, bended, twisted, folded, and compressed, representing that f-PVA3 maintains superior mechanical flexibility at the frozen temperature. Figure S7 exhibits tensile stress-strain cycling curves of f-PVA3 at RT and −40 °C, and the results indicate that the f-PVA3 has fatigue resistance within a certain range and the cold environment enhances mechanical stress. The compressive strain curves of f-PVA3 in Figure S8 also demonstrate that f-PVA3 remains an excellent elasticity at RT, but decreasing at −40 °C. Therefore, it can be confirmed that a freeze-dried hydrogel with the concentrated electrolyte has an excellent flexibility and mechanical strength in an extremely low temperature, which is suitable for quasi-solid-state supercapacitors working at a wide temperature range.

In order to ensure the electrolyte ions migration at low temperatures, the freezing point of f-PVA3 was firstly probed by the DSC, and the result of f-PVA3 is shown in Figure 2(a). The lowest freezing point of the sample is −51.14 °C illustrating that electrolyte ions can be transport in a frigid environment. It can be inferred that the PANi-f-PVA3 supercapacitor can maintain electrochemical activity at low temperatures benefiting from the f-PVA3 hydrogel. In order to quantify the ionic conductivity, the EIS was conducted on the f-PVA with different concentrated H_2SO_4 at low temperatures in the frequency range of 10^5–10^{-2} Hz (Figure 2(b)). The values of ionic conductivity are calculated according to the Eq. (S1) (Supporting Information online). At RT, the ionic conductivities of f-PVA1, f-PVA2, and f-PVA3 increase with the increasing concentration of H_2SO_4 solutions. Then the values decline when the operation temperature goes down to −40 °C, but that of f-PVA3 gel slightly increases at −20 °C. Previous studies [31,32] reported that the low temperature can boost the dissociation of H_2SO_4, so that more protons can be obtained from the ionizing H_2SO_4 and HSO_4^-. From Figure 2(c), the relationship of the square root of frequency ($\omega^{-1/2}$) with the real part of impedance (Z') shows that the f-PVA3 has a lower slope than f-PVA1 and f-PVA2, denoting fast ions migration in the f-PVA3 gel. However, the slope of f-PVA3 increases with the reducing temperature, illustrating that the frozen temperature is adverse for the electrolyte ions transport (Figure 2(d)). Although the ionic conductivity of f-PVA3 at −40 °C (5.92 mS cm^{-1}) is significantly lower than that of f-PVA3 at RT (57.5 mS cm^{-1}), it is comparable to various published hydrogels based on different non-aqueous electrolytes (Table S1, Supporting Information online). Thus, the anti-freezing hydrogel can be fabricated in a simple and scalable method and behaves good mechanical flexibility and superior ionic conductivity at −40 °C.

In order to study the improvement effected by f-PVA3 hydrogel, we fabricated an all-in-one integrated quasi-solid-state supercapacitor and the electrochemical properties of samples were measured at different temperatures. According to the step (ii) and step (iii) in Figure S1, PANi electrodes were *in situ* polymerized on the f-PVA film. Then the PANi-f-PVA3 capacitor was obtained by cutting edges of the resulted film and immersing in 3 mol L^{-1} H_2SO_4 solution for

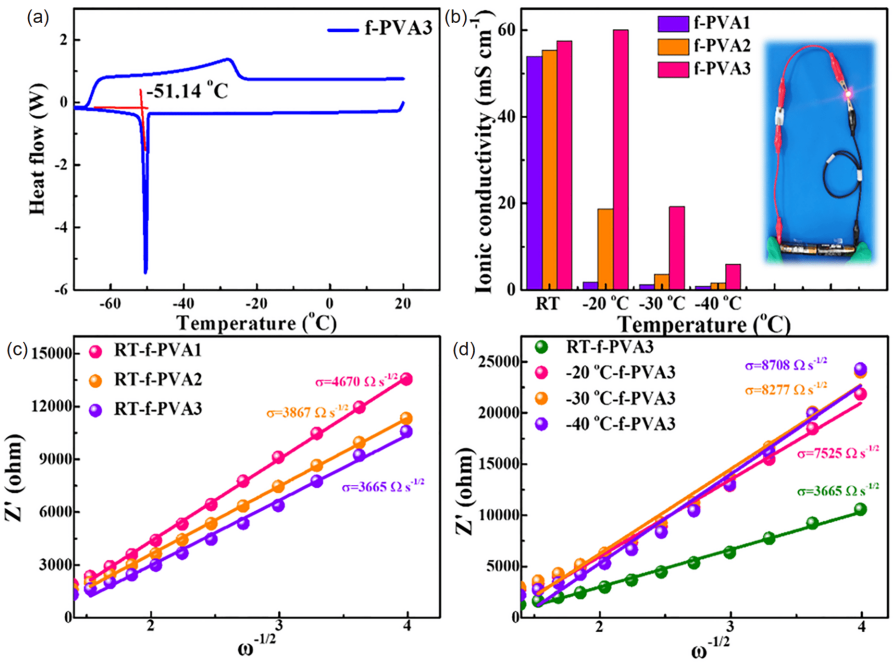

Figure 2 (a) DSC for f-PVA3; (b) temperature-dependent ionic conductivity (the inset shows f-PVA3 gel serves as a conductor to connect an LED circuit); (c, d) relationship between Z' and $\omega^{-1/2}$ (color online).

24 h. The morphologies of the supercapacitor were characterized by SEM, and the results are shown in Figure 3(a, b). After loading PANi electrode materials, the surface becomes relatively rough, and the cross-section image of the supercapacitor shows a typical sandwich structure. EDS mapping in Figure S9 shows that PANi electrodes are uniformly polymerized on both sides of the gel. FT-IR spectra show that the peaks located in 1,485 and 1,201 cm^{-1} are assigned to C=C and C=N stretching vibrations derived from PANi, and the peak near 3,349 cm^{-1} is attributed to –OH groups from PVA (Figure 3(c)) [33]. Besides, after ultrasonic cleaning in deionized water for 1 h, the resulting solution keeps clear (Figure S6(c)). Moreover, the tearing tests in Figure S6(d) show that no PANi is attached to the tape, demonstrating that PANi electrodes are tightly coated on f-PVA hydrogel.

After immersing in 3 mol L^{-1} H_2SO_4 solutions for 24 h, the electrochemical performance of f-PVA3 capacitor was investigated by CV, GCD and EIS at low temperatures. Firstly, according to Figure S10, the PANi-f-PVA3 capacitor has a high area capacitance (298.6 mF cm^{-2} and 26.5 F g^{-1} at 0.5 mA cm^{-2}) and superior rate performance (maintain 69% at 50 mA cm^{-2}) when the sample was fabricated in 0.4 mol L^{-1} aniline monomers solution. In order to study the electrochemical behaviors of the capacitors at low temperature, all samples in following research work were synthesized in 0.4 mol L^{-1} aniline monomers solution. CV tests were firstly performed on PANi-f-PVA1, PANi-f-PVA2, and PANi-f-PVA3 in the two-electrode system with a voltage of 0.8 V. Figure 3(d) shows the CV curves of three capacitors at sweep rate of 1 mV s^{-1} at RT, and the redox peaks in the voltage range of 0.2–0.5 V are attributed to the pseudocapacitance of PANi during the charge/discharge process. The integral area enclosed by the CV curve of all-in-one capacitors slightly increase with the increasing concentration of the soaked H_2SO_4 electrolyte, which implies that the capacitance increases with the increase of electrolyte concentration. When the temperature drops to −40 °C, Figure 3(e) shows that the enclosed area of PANi-f-PVA3 decreases slightly, however, that of PANi-f-PVA1 dramatically reduces (Figure S11(a)). It demonstrates that the PANi-f-PVA3 capacitor has a better electrochemical performance than PANi-f-PVA1 at −40 °C. Increasing the scan rate to 50 mV s^{-1}, the enclosed area of PANi-f-PVA3 is larger than the others in Figure 3(f), denoting that PANi-f-PVA3 has a high specific capacitance and favorable rate performance at −40 °C. In light of the GCD results shown in Figure S12, the curves of three samples display an approximately symmetric triangular shape indicating a fast and reversible charge/discharge process. And the area capacitance of PANi-f-PVA1, PANi-f-PVA2, and PANi-f-PVA3 are 278.8, 294.4, and 296.9 mF cm^{-2}, respectively. When measured at −40 °C, PANi-f-PVA1 delivers 207.6 mF cm^{-2} accounting for 74.5% of the capacitance at RT. Meanwhile, the capacitance of PANi-f-PVA2 is 228.1 mF cm^{-2} (retains 77.5%), and that of PANi-f-PVA3 is 278.6 mF cm^{-2} (retains 93.8%) as shown in Figure S12(a, b). As the current density increases to 10 mA cm^{-2}, the capacitance of three samples are approx-

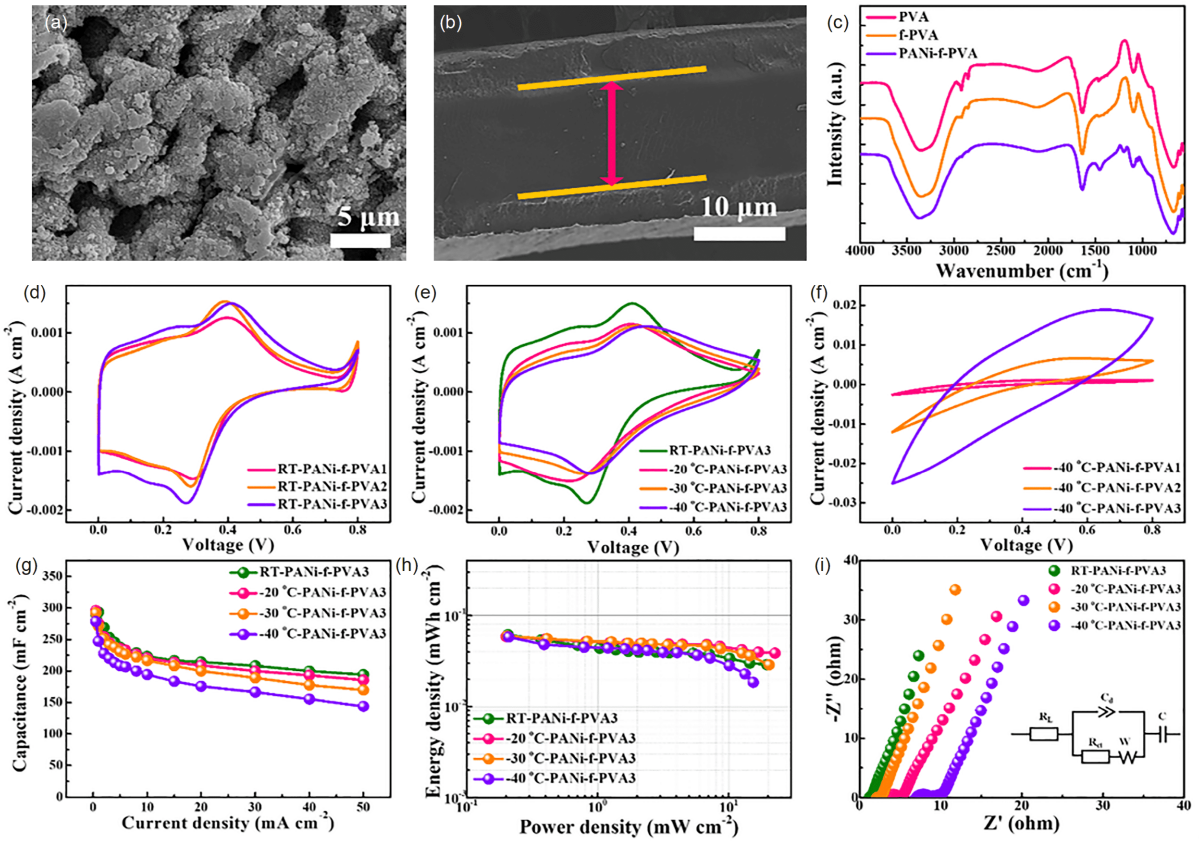

Figure 3 SEM images of PANi-f-PVA3 (a) surface and (b) cross-section. (c) FT-IR spectra. Electrochemical performance: (d) CV curves at a scan rate of 1 mV s^{-1} at RT; (e) CV curves of PANi-f-PVA3 at 1 mV s^{-1} at different temperatures; (f) CV curves at a sweep rate of 50 mV s^{-1} at −40 °C. (g) Rate performance of PANi-f-PVA3 at different temperatures. (h) Ragone plots. (i) Nyquist plots (color online).

imative at RT as shown in Figure S12(c). At −40 °C, however, the PANi-f-PVA3 can offer more energy than the other capacitors (Figure S12(d)). What's more, the specific capacitance of PANi-f-PVA3 remains 50% as the current density increases from 0.5 to 50 mA cm^{-2} at −40 °C, while PANi-f-PVA1 and PANi-f-PVA2 just keep 1% and 5%, respectively (Figure 3(g) and S13). The results confirm that the freezing-tolerant hydrogel with high ionic conductivity promotes the PANi-f-PVA3 supercapacitor exhibiting an excellent electrochemical performance at low temperatures. To our best knowledge, the all-in-one supercapacitor exhibits an excellent energy density (0.058 mW h cm^{-2}), and high-power density (15.4 mW cm^{-2}) at −40 °C, and the electrochemical properties of PANi-f-PVA3 are close to those of low-temperature resistant supercapacitors, which are configured with ionic liquid-based electrolyte or organic hydrogel-based solid electrolyte (Figure 3(h) and Table S2) [2,14,15]. In addition to PANi, some other conductive polymers (such as PPy) are used as electrodes to fabricate the low-temperature resistant supercapacitor with f-PVA3 as electrolyte. Figure S14 contrasts the electrochemical properties of PPy-f-PVA1 and PPy-f-PVA3 at low temperature. The results certificate that f-PVA3 gels improve the low temperature properties of quasi-solid-state capacitors.

To understand the charge transport behavior at low temperatures, EIS measurements were performed on PANi-f-PVA3 within an ac perturbation of 5 mV at different temperatures. Figure 3(i) shows the Nyquist plots which consist of a semicircle arc and a straight line corresponding to the charge-transfer resistance at high-frequency regions and the ion-diffusion resistance obtained from the low-frequency regions, respectively. According to the equivalent circuit in Figure 3(i), the charge-transfer resistance (R_{ct}) of PANi-f-PVA3 is 1.8 Ω at RT and increases to 5 Ω at −40 °C [1,11,34]. The relationship between Z' and $\omega^{-1/2}$ in Figure S15 represents the ion-diffusion capability of quasi-solid-state supercapacitors. The higher slope of PANi-f-PVA3 means that the electrolyte ions behave sluggish migration at −40 °C. What's more, in the Bode plots, the frequency corresponding to the phase angle of −45° is used to calculate the relaxation time constant (τ_0) [3]. Normally, τ_0 is related to the percentage of available capacitance energy, which means that the smaller τ_0 relates to the fast current response. The τ_0 values at different temperatures are 3.8 s (RT), 8.3 s (−20 °C), 10 s (−30 °C), and 31.6 s (−40 °C), respectively (Figure S16). It explains that PANi-f-PVA3 has a slow current response at −40 °C. Thus, the above results indicate that due to the increasing charge transfer resistance and sluggish

ion diffusion in the cold environment, the current response behavior of the capacitor becomes slower, so that the specific capacitance decreases and the rate performance deteriorates.

The energy storage mechanism at low temperatures is studied by comparing the capacitive contribution of the PANi-f-PVA3 at RT and low temperatures. Normally, CV curves at different scan rates are used to analyze the capacitive contribution during electrochemical reaction by the follow Eq. (1) as follows:

$$i = av^b \quad (1)$$

where i is current response, v is sweep rate, a and b are two adjustable constants. What's more, the b-value can be calculated by drawing lg$i$-lg$v$ linear plots as follow [35]:

$$\lg i = b\lg v + \lg a \quad (2)$$

where b=1 signifies the electric double-layer capacitance/pseudocapacitance, while b=0.5 represents the diffusion-controlled process [36–38]. Figure 4(a) shows that the b-values at different potentials are in a range of 0.5–1, indicating that the capacitive storage is manipulated by both capacitive behavior and ion diffusion [39]. In view of this, the percentage of capacitive contribution is further calculated by the Eq. (3) as follows:

$$i = k_1v + k_2v^{1/2} \quad (3)$$

where k_1v and $k_2v^{1/2}$ are corresponding to the surface capacitance from the interface of PANi and gel electrolyte and the diffusion-controlled effect from PANi electrodes, respectively [30,39]. Figure 4(b) and Figure S13 show the variation of capacitive contribution with scanning rates at −40 °C, where the red shaded region represents the surface capacitance. The normalized capacitive contribution percentage as a function of sweep rate for PANi-f-PVA3 capacitor is shown in Figure 4(c, d). It can be observed that the ratio of surface capacitance to the total capacitance increases with the increasing sweep rates at RT and −40 °C. However, as the scanning rates increase from 1 to 50 mV s^{-1}, the surface contribution at RT increased by 51.0%, while it increased by 35.6% at −40 °C. Figures S17 and S18 also show that the surface capacitance has a higher ratio at RT. According to the EIS results in Figure 2(d), it can be inferred that the slow ion migration at low temperature leads to a less increase of the

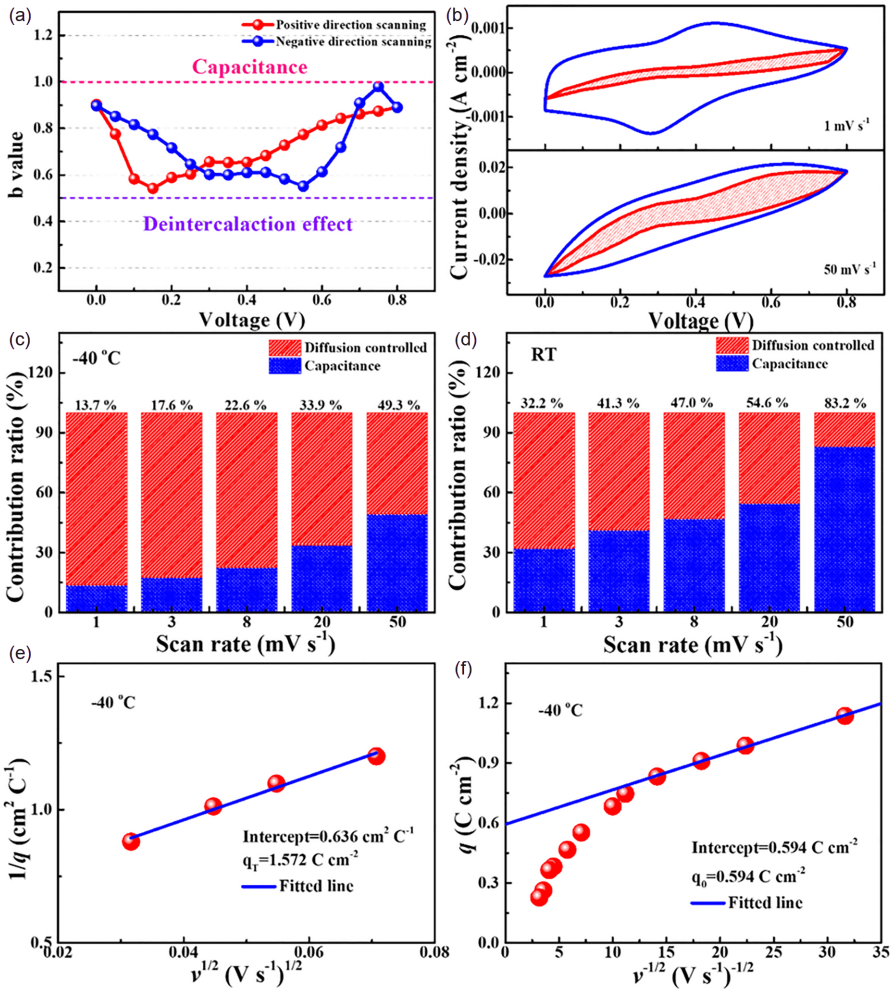

Figure 4 (a) b-values against the voltage at −40 °C; (b) capacitive contribution at −40 °C under different sweep rates; (c) capacitive contribution at −40 °C; (d) capacitive contribution at RT; (e) q^{-1} *vs.* $v^{1/2}$; (f) q *vs.* $v^{-1/2}$ (color online).

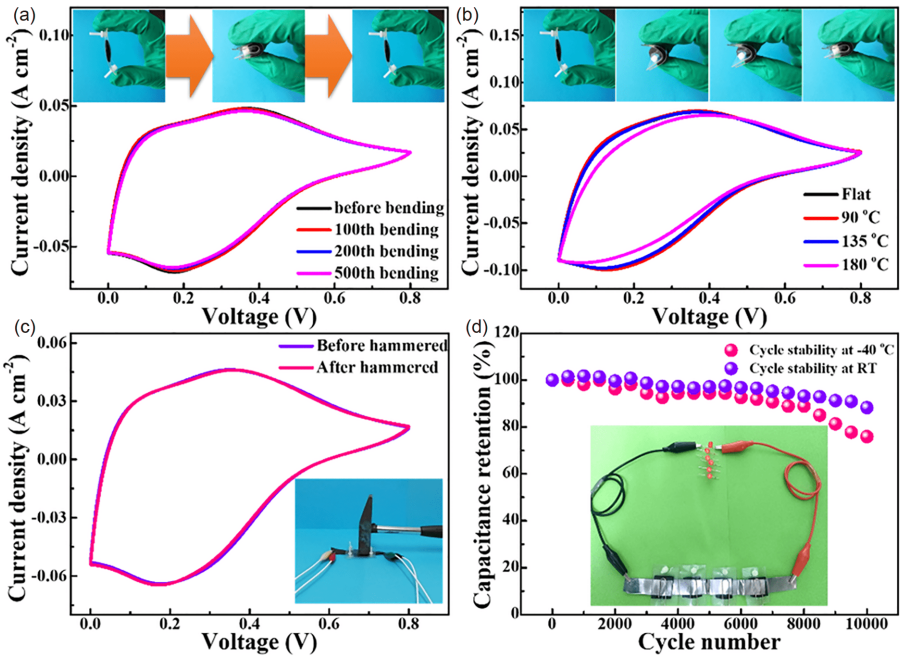

Figure 5 (a) CV curves at 30 mV s^{-1} after bending multiple times; (b) CV curves at 50 mV s^{-1} under different bending angles; (c) CV curves at 30 mV s^{-1} before and after hammered; (d) cycle stability (inset is a digital graphe of LED powered by four units devise) (color online).

percentage of surface capacitance. Thus, the results indicate that the capacitance of PANi-f-PVA3 at low temperature is more derived from the Faraday reaction.

To investigate the charge storage at the frozen environment, the Trasatti analysis method was carried out to quantify the stored charges, including the outer surface charge (q_o) which is easy for ions accessing and the inner surface charge (q_i) which is hard for electrolyte ions to approach [40,41]. The total stored charge (q_T) is calculated as follows:

$$q_T = q_i + q_o \quad (4)$$

Generally, the charge storage at the outer face is not controlled by diffusion so that the variation of q_o is not related to scanning rates, yet the charge storage at the inner face is controlled by the diffusion process [41]. Thus, the value of q_T has a function of sweep rate (v) as follows:

$$q(v) = q_\infty + kv^{-1/2} \quad (5)$$

where $kv^{-1/2}$ is corresponding to the charge storage of semi-infinite diffusion. In light of the dependence of q^{-1} on $v^{1/2}$ shown in Figure 4(e), the number of outer charges (q_o =0.594 C cm^{-2}) was obtained by extrapolating q to $v\rightarrow\infty$, while the extrapolation q to v=0 in Figure 4(f) derives the total stored charges (q_T=1.572 C cm^{-2}). Thus, the surface stored charges account for 20% of q_T indicating that the specific capacitance of PANi-f-PVA3 is mainly from the diffusion process in electrodes in the cold environment. Furthermore, Figure S19 shows that the number of q_o at RT is 0.686 C cm^{-2}, while q_T is 1.992 C cm^{-2}. Therefore, the charge storage of PANi-f-PVA3 is mainly from the Faraday reaction of PANi, so that the decrease in ionic conductivity has little effect on the electrochemical performance of the capacitor at low temperatures.

The electrochemical stability on deformation states were further investigated by CV tests (Figure 5(a, b)). On one hand, the CV curves of PANi-f-PVA3 capacitor tested at 30 mV s^{-1} show negligible change after bending multiple times. On the other hand, the CV curves at the different bending angles are close to that in flat state. It demonstrates that the all-in-one supercapacitor has good electrochemical stability under deformed conditions. Additionally, the similar CV curves tested before and after hammered illustrate that the as-prepared quasi-solid-state supercapacitor is able to resist mechanical impact (Figure 5(c)). To evaluate the electrochemical stability of PANi-f-PVA3, GCD was conducted at RT and −40 °C for 10,000 cycles, and the results are shown in Figure 5(d). After 10,000 charging/discharging cycles, the capacitor retains 88.27% and 75.92% of the initial capacitance at RT and −40 °C, respectively. Comparing the SEM images of Figure 3(a) and Figure S17, it can be inferred that PANi electrodes are instable during the charging and discharging process due to the volume expansion and contraction, thereby reducing the performance of the capacitor. In addition, the inset in Figure 5(d) and the supplementary movie certificate the practical application of the device.

4 Conclusions

In this work, a facile and scalable strategy is developed to fabricate the freezing-tolerant f-PVA hydrogel with several

advantages of exceptional ionic conductivity (5.92 mS cm^{-1} at −40 °C), a low freezing point (−51.14 °C), and superior flexibility at −40 °C. Thus, the PANi-f-PVA3 supercapacitor displays the excellent electrochemical properties at the subzero temperature assembled by the anti-freezing hydrogel electrolyte. In the frosty environment of −40 °C, PANi-f-PVA3 delivers high specific capacitance of 278.6 mF cm^{-2} at 0.5 mA cm^{-2} (accounting for 93.8% of the capacitance at RT), good rate performance (50% retention at 50 mA cm^{-2}), and superb electrochemical stability (retaining 88.9% of the initial capacitance after 8,000 cycles). Moreover, the all-in-one configured supercapacitor delivers a fair power density (15.36 mW cm^{-2}) and energy density (0.058 mW h cm^{-2}). Given the above attributes, the cold resistance hydrogels hold great promise for a wide application prospect in portable energy storage devices.

Acknowledgements This work was supported by the Major Science and Technology Projects of Heilongjiang Province (2019ZX09A01) and the National Key Technology R&D Program (2017YFB1401805).

Conflict of interest The authors declare no conflict of interest.

Supporting information The supporting information is available online at http://chem.scichina.com and http://link.springer.com/journal/11426. The supporting materials are published as submitted, without typesetting or editing. The responsibility for scientific accuracy and content remains entirely with the authors.

1 Xu J, Yuan N, Razal JM, Zheng Y, Zhou X, Ding J, Cho K, Ge S, Zhang R, Gogotsi Y, Baughman RH. *Energy Storage Mater*, 2019, 22: 323–329
2 Yang Y, Ng SW, Chen D, Chang J, Wang D, Shang J, Huang Q, Deng Y, Zheng Z. *Small*, 2019, 15: 1902071
3 Lin Y, Zhang H, Liao H, Zhao Y, Li K. *Chem Eng J*, 2019, 367: 139–148
4 Zhou Y, Wang CH, Lu W, Dai L. *Adv Mater*, 2020, 32: 1902779
5 Yang C, Pan Q, Jia Q, Xin Y, Qi W, Wei H, Yang S, Cao B. *Appl Surf Sci*, 2020, 502: 144423
6 Lv T, Liu M, Zhu D, Gan L, Chen T. *Adv Mater*, 2018, 30: 1705489
7 Mo F, Liang G, Meng Q, Liu Z, Li H, Fan J, Zhi C. *Energy Environ Sci*, 2019, 12: 706–715
8 Sui X, Guo H, Chen P, Zhu Y, Wen C, Gao Y, Yang J, Zhang X, Zhang L. *Adv Funct Mater*, 2020, 30: 1907986
9 Jiang H, Shin W, Ma L, Hong JJ, Wei Z, Liu Y, Zhang S, Wu X, Xu Y, Guo Q, Subramanian MA, Stickle WF, Wu T, Lu J, Ji X. *Adv Energy Mater*, 2020, 10: 2000968
10 Peng X, Liu H, Yin Q, Wu J, Chen P, Zhang G, Liu G, Wu C, Xie Y. *Nat Commun*, 2016, 7: 11782
11 Xu J, Wang X, Zhou X, Yuan N, Ge S, Ding J. *Electrochim Acta*, 2019, 301: 478–486
12 Lang J, Zhang X, Liu L, Yang B, Yang J, Yan X. *J Power Sources*, 2019, 423: 271–279
13 Wu QL, Zhao SX, Yu L, Zheng XX, Wang YF, Yu LQ, Nan CW, Cao G. *J Mater Chem A*, 2019, 7: 13205–13214
14 Jin X, Zhang G, Sun G, Yang H, Xiao Y, Gao J, Zhang Z, Jiang L, Qu L. *Nano Energy*, 2019, 64: 103938
15 Rong Q, Lei W, Huang J, Liu M. *Adv Energy Mater*, 2018, 8: 1801967
16 Wu J, Wu Z, Lu X, Han S, Yang BR, Gui X, Tao K, Miao J, Liu C. *ACS Appl Mater Interfaces*, 2019, 11: 9405–9414
17 Hu C, Zhang Y, Wang X, Xing L, Shi L, Ran R. *ACS Appl Mater Interfaces*, 2018, 10: 44000–44010
18 Nian Q, Wang J, Liu S, Sun T, Zheng S, Zhang Y, Tao Z, Chen J. *Angew Chem Int Ed*, 2019, 58: 16994–16999
19 Pei Z, Yuan Z, Wang C, Zhao S, Fei J, Wei L, Chen J, Wang C, Qi R, Liu Z, Chen Y. *Angew Chem Int Ed*, 2020, 59: 4793–4799
20 Abbas Q, Béguin F. *J Power Sources*, 2016, 318: 235–241
21 Liu Z, Zhang J, Liu J, Long Y, Fang L, Wang Q, Liu T. *J Mater Chem A*, 2020, 8: 6219–6228
22 Zhang XF, Ma X, Hou T, Guo K, Yin J, Wang Z, Shu L, He M, Yao J. *Angew Chem Int Ed*, 2019, 58: 7366–7370
23 Morelle XP, Illeperuma WR, Tian K, Bai R, Suo Z, Vlassak JJ. *Adv Mater*, 2018, 30: 1801541
24 Lu X, Yu M, Wang G, Tong Y, Li Y. *Energy Environ Sci*, 2014, 7: 2160
25 Wang K, Zhang X, Li C, Sun X, Meng Q, Ma Y, Wei Z. *Adv Mater*, 2015, 27: 7451–7457
26 Wang Y, Lv C, Ji G, Hu R, Zheng J. *J Mater Chem A*, 2020, 8: 8255–8261
27 Kumar A, Mishra R, Reinwald Y, Bhat S. *Mater Today*, 2010, 13: 42–44
28 Su L, Gong L, Lü H, Xü Q. *J Power Sources*, 2014, 248: 212–217
29 Zhang H, Xia H, Zhao Y. *ACS Macro Lett*, 2012, 1: 1233–1236
30 Bai Y, Liu R, Wang Y, Xiao H, Liu Y, Yuan G. *ACS Appl Mater Interfaces*, 2019, 11: 43294–43302
31 Knopf DA, Luo BP, Krieger UK, Koop T. *J Phys Chem A*, 2003, 107: 4322–4332
32 Mund C, Zellner R. *ChemPhysChem*, 2003, 4: 638–645
33 Chu X, Huang H, Zhang H, Zhang H, Gu B, Su H, Liu F, Han Y, Wang Z, Chen N, Yan C, Deng W, Deng W, Yang W. *Electrochim Acta*, 2019, 301: 136–144
34 Lai F, Feng J, Yan R, Wang GC, Antonietti M, Oschatz M. *Adv Funct Mater*, 2018, 28: 1801298
35 Zhao S, Dong L, Sun B, Yan K, Zhang J, Wan S, He F, Munroe P, Notten PHL, Wang G. *Small*, 2020, 16: 1906131
36 Wang J, Polleux J, Lim J, Dunn B. *J Phys Chem C*, 2007, 111: 14925–14931
37 Brezesinski T, Wang J, Tolbert SH, Dunn B. *Nat Mater*, 2010, 9: 146–151
38 Li K, Wang X, Li S, Urbankowski P, Li J, Xu Y, Gogotsi Y. *Small*, 2020, 16: 1906851
39 Chen S, Zhang Y, Geng H, Yang Y, Rui X, Li CC. *J Power Sources*, 2019, 441: 227192
40 Wang Y, Wang X, Li X, Bai Y, Xiao H, Liu Y, Liu R, Yuan G. *Adv Funct Mater*, 2019, 29: 1900326
41 Yan J, Ren CE, Maleski K, Hatter CB, Anasori B, Urbankowski P, Sarycheva A, Gogotsi Y. *Adv Funct Mater*, 2017, 27: 1701264